

Article

# Improvement of Sensing Performance of Impedancemetric C<sub>2</sub>H<sub>2</sub> Sensor Using SmFeO<sub>3</sub> Thin-Films Prepared by a Polymer Precursor Method

Tomohisa Tasaki, Satoko Takase and Youichi Shimizu \*

Department of Applied Chemistry, Kyushu Institute of Technology, 1-1 Sensui-cho, Tobata, Kitakyushu 804-8550, Fukuoka, Japan; takky0726@gmail.com (T.T.); satoko@che.kyutech.ac.jp (S.T.)

\* Correspondence: shimizu.youichi366@mail.kyutech.jp; Tel.: +81-93-884-3323

Received: 27 December 2018; Accepted: 8 February 2019; Published: 13 February 2019



**Abstract:** A sensitive an impedancemetric acetylene (C<sub>2</sub>H<sub>2</sub>) gas sensor device could be fabricated by using perovskite-type SmFeO<sub>3</sub> thin-film as a sensor material. The uniform SmFeO<sub>3</sub> thin-films were prepared by spin-coating and focusing on the effects of polymer precursor solutions. The prepared precursors and thin-films were characterized by means of thermal analysis, Fourier-transform infrared spectroscopy, ultraviolet–visible spectroscopy, X-ray diffraction analysis, scanning electron microscopy and X-ray photoelectron spectroscopy. It was found that particle growth and increase in homogeneity of the prepared thin-film could be accelerated by the addition of acetyl acetone (AcAc) as a coordination agent in the polymer precursor solution. Moreover, the highly crystallized thin-film-based sensor showed good response properties and stabilities to a low C<sub>2</sub>H<sub>2</sub> concentration between 0.5 and 2.0 ppm.

**Keywords:** perovskite-type oxide; thin-film; polymer precursor; acetyl acetone; gas sensor; AC impedance; acetylene

## 1. Introduction

Hydrocarbon gases are mostly toxic and flammable; for example, automobile exhaust and industrial plant soot contain carbon monoxide (CO), nitrogen oxide (NO<sub>x</sub>) and hydrocarbons (HCs) which cause various environmental issues. In the agro-food field, ethylene (C<sub>2</sub>H<sub>4</sub>) is known as a growth hormone for vegetables and fruits [1,2]. C<sub>2</sub>H<sub>2</sub>, the detection gas in this study, is also an important industrial gas, which has been used in the field of synthetic chemistry as a starting material of benzene and poly-acetylene. Recently, it is known that C<sub>2</sub>H<sub>2</sub> is generated from the insulating oil of transformers when the oil becomes deteriorated. Therefore, a C<sub>2</sub>H<sub>2</sub> sensor should be used for on-site monitoring of the transformer, in spite of the generated C<sub>2</sub>H<sub>2</sub> having a low concentration of 0.5 ppm or lower [3–5]. Thus, studies about C<sub>2</sub>H<sub>2</sub> sensors have recently increased in number due to the importance of C<sub>2</sub>H<sub>2</sub> detection.

Perovskite-type oxides, which are functional inorganic materials, have a wide range of applications and various interesting properties, including ion conductivity [6] and catalytic activity [7]. The perovskite-type oxide is also used as a good sensor material, and has displayed sensing properties toward various harmful gases, such as NO<sub>x</sub> [8], VOC [9], NH<sub>3</sub> [10], CO [11] and hydrocarbons [12].

In this study, we focused on a semiconductive gas sensor based on a perovskite-type oxide, because of its good sensitivity and long stability. In the sensing function of a semiconductive gas sensor using oxide materials, it is important to discuss chemical adsorption over the oxide surface, because sensor response shows a similar behavior to a catalyst. Many research results of density functional theory of CO adsorption properties for Fe-based perovskite oxides have been reported, and this way of

thinking could improve the sensor properties because the electron orbital state (HOMO–LUMO) of B-site metal of the  $\text{BO}_6$  octahedral ion influences many chemical properties [13–15]. In fact, we have reported that the  $\text{SmFeO}_3$  thin-film is the only sensor material to have high sensitivity and selectivity to  $\text{C}_2\text{H}_2$  among the prepared  $\text{SmBO}_3$  ( $\text{B}=\text{Cr, Mn, Fe, Co}$ ) thin-films [16,17]. Therefore, we are currently researching the response mechanism from a standpoint of HOMO–LUMO energy interaction between the oxide and  $\text{C}_2\text{H}_2$ .

By the way, the use of an oxide thin-film would give higher sensitivity and performance, and there are many ways to obtain a homogeneous and good crystalline thin-film [18–23].

In this study, we tried to synthesise perovskite-type thin-films by a wet-chemical route using a polymer precursor method prepared by adjustment of the additive amount of AcAc as a coordination agent in the precursor. The  $\text{C}_2\text{H}_2$  sensing properties of the devices and the mechanism were discussed. We have developed a highly sensitive  $\text{C}_2\text{H}_2$  sensor device.

## 2. Materials and Methods

### 2.1. Preparation and Analysis of Precursor and Oxide Thin-Film

Figure 1 shows the process of preparation of the perovskite-type oxide  $\text{SmFeO}_3$  thin-film by a polymer precursor method, in which stoichiometric amounts of metal nitrates,  $\text{Sm}(\text{NO}_3)_3 \cdot 6\text{H}_2\text{O}$  and  $\text{Fe}(\text{NO}_3)_3 \cdot 9\text{H}_2\text{O}$  ( $0.5 \text{ mol} + 0.5 \text{ mol} = \text{A mol}$ ) were dissolved in ethylene glycol (EG; 5 mL) solvent. Then, multiples of 2-, 4- and 8-times the solvent amount of acetyl acetone (AcAc; 2A, 4A and 8A mol, respectively) and polyvinylpyrrolidone (PVP; 3.75 wt % of total materials) as a coordination agent and a polymer additive, respectively, were added to this solution. The solutions were abbreviated as AcAcX, in which X is the mol content of acetyl acetone ( $X = 0, 2, 4, 8$ ). The AcAc0 means a solution without AcAc. The prepared precursor solutions were spin-coated on an alumina substrate with Au interdigitated electrodes at 4000 rpm, and finally sintered at  $750^\circ\text{C}$  for 2 h in air. The spin-coating and sintering processes were repeated 3 times [16] to avoid making cracks.

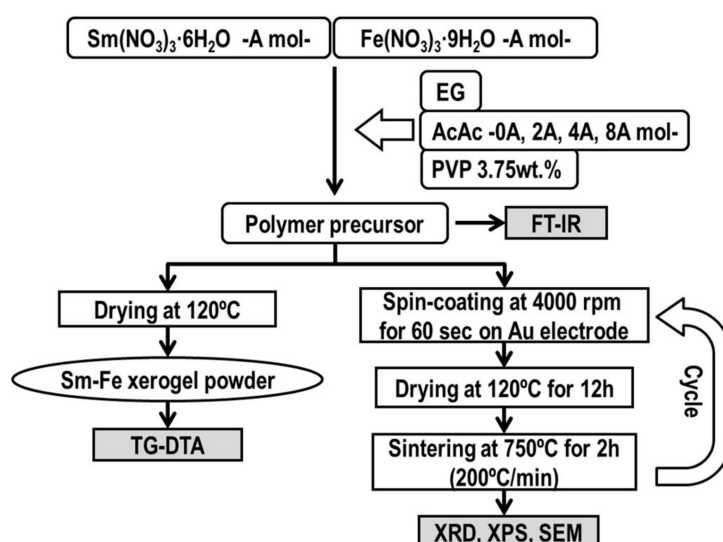


Figure 1. Flowchart for preparation route of perovskite-type oxide  $\text{SmFeO}_3$  thin-films.

Characterizations of the prepared materials were carried out by means of the following methods; Fourier-transform infrared spectroscopy (FT-IR, IRPrestige-21, Shimadzu, Kyoto, Japan), ultraviolet–visible spectroscopy (UV-Vis, U-3900, Hitachi, Kyoto, Japan), thermogravimetric–differential thermal analysis (TG-DTA, TG-8120, Rigaku, Japan), and X-ray diffraction analysis (XRD, JDX3500K, JEOL, Kyoto, Japan) using  $\text{CuK}\alpha$  radiation. Surfaces of the thin-films were analyzed by a scanning electron microscope (SEM, JSM-6701, JEOL, Kyoto, Japan) and X-ray photoelectron spectroscopy

(XPS, Axis-Nova, Shimadzu Kratos, Kyoto, Japan) using Al K $\alpha$  radiation, and all binding energy values were calibrated with the C<sub>1s</sub> line at 284.5 eV.

## 2.2. Measurement of Sensing Properties

The measurement apparatus and the sensor device are shown in Figure 2. The sensor device was attached to a gold wire ( $\phi = 0.3$  mm) with Ag paste and connected to an LCR meter (HIOKI 3532-50). Gas sensing properties of the device were investigated by an AC impedance method with an applied voltage of 0.5 V at the frequency range between 50 Hz and 5 MHz. Measurement temperatures were used between 300 and 500 °C. Gas concentration was controlled by mixing with dry synthetic C<sub>2</sub>H<sub>2</sub> + N<sub>2</sub> parent gas mixture, dry synthetic air (N<sub>2</sub> and O<sub>2</sub>), N<sub>2</sub>, and O<sub>2</sub> at a fixed concentration of P<sub>O<sub>2</sub></sub> = 0.21 atm under a gas flow rate of 100 cm<sup>3</sup>/min.

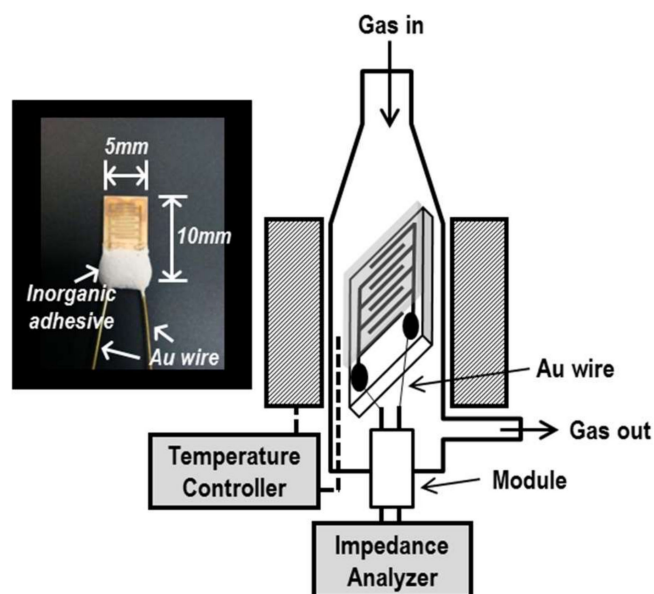


**Figure 2.** Schematic diagrams of the measurement apparatus and the actual image of the oxide thin-film device.

## 3. Results and Discussion

### 3.1. Preparation of the Precursor Solutions

To investigate effects of AcAc addition for the precursor, thermal behavior was firstly measured. Figure 3 shows TG–DTA curves of the precursor powders prepared by drying at 120 °C. In the case of the AcAc0 powder, the DTA curve showed a large exothermic reaction with a weight loss (ca. 40%) at ca. 180 °C, which corresponds to the pyrolysis of remaining EG and nitrates of the starting materials. However, all DTA curves of precursors with AcAc indicated different exothermic reactions, that is, a weight loss (ca. 10%) was indicated at ca. 210 °C instead of diminishing the pyrolysis at 180 °C. This reaction might be due to a pyrolysis of the excess amounts of AcAc. Moreover, the TG–DTA curves showed a large exothermic peak with 10% weight loss at ca. 320 °C, leaving a complex of EG and AcAc linked like a polymer with metal cations formed in the precursor under heat conditions [21]. There is, furthermore, a large pyrolysis divided into two peaks at 420–440 °C. Both reactions could be assigned to the decomposition of the complex network and the combustion of PVP, respectively.

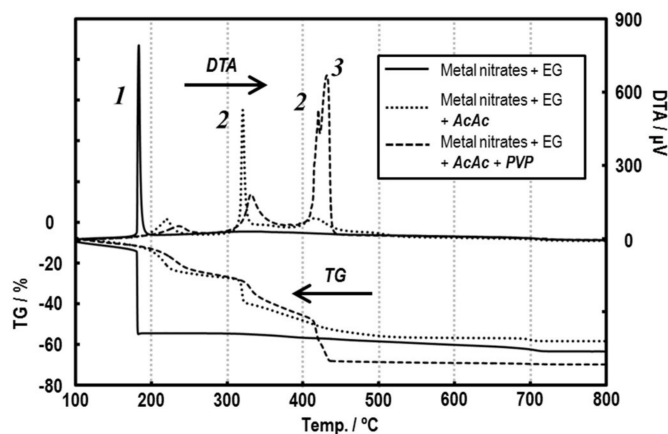


Figure 3. TG-DTA curves of Sm-Fe precursors dried at 120 °C.

FT-IR spectra of the solutions are shown in Figure 4. The peak #3, which could be assigned to the presence of a carboxylic (C=O) stretch peak from AcAc, appears at  $1705\text{ cm}^{-1}$  in Figure 4g [19,23]. In Figure 4f, the peak that shifted from  $1705\text{ cm}^{-1}$  to  $1697\text{ cm}^{-1}$  could seem to be a link between metal cations and carboxylic oxygen, and this brought about an increase in the moment of the bond from the relation between energy and wavelength [19]. Peak #4 at  $1523\text{ cm}^{-1}$  appeared after adding metal nitrates in AcAc, which could be attributed to the bond between both materials [24]. The peaks #1 at  $1242$  and  $1357\text{ cm}^{-1}$  and the peaks #2 at  $1415$  and  $1612\text{ cm}^{-1}$  were attributed to the asymmetric vibration of the carbon chain of AcAc and C=O stretching modes, respectively. The two strong peaks #5 at  $1037$  and  $1083\text{ cm}^{-1}$  also corresponded to C–O stretching of primary and secondary alcohols [22]. Additionally, these phenomena could be corroborated by UV-Vis spectra due to a broad peak for a d–d electron transition and a shoulder peak for a charge-transfer transition at ca. 450 and 350 nm, respectively.

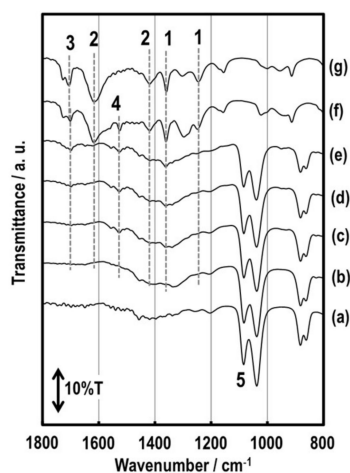


Figure 4. FT-IR spectra of the various solutions and the Sm-Fe precursor solutions without PVP; (a) EG only, (b) AcAc0, (c) AcAc2, (d) AcAc4, (e) AcAc8, (f) metal nitrates with AcAc, and (g) AcAc only.

### 3.2. Structure of the $\text{SmFeO}_3$ Thin-Films

Figure 5 shows XRD patterns of oxide thin-films sintered at  $750\text{ °C}$  for 2 h. The oxide thin-films showed almost single-phase perovskite-type  $\text{SmFeO}_3$ , and the peak intensities increased with increasing the amounts of AcAc. It could be seen that AcAc accelerates crystal growth of the oxides. Figure 6 shows SEM images of the  $\text{SmFeO}_3$  thin-films prepared by AcAc0, 2, 4 and 8 precursors sintered at  $750\text{ °C}$ . We can see an increase in particle size of the  $\text{SmFeO}_3$  thin-film with increasing amounts of

AcAc. Particles of the AcAc8 film seemed to clump together, although grain size of the AcAc8 film was smaller than that of the AcAc4 film. However, there is no large difference in film thickness.

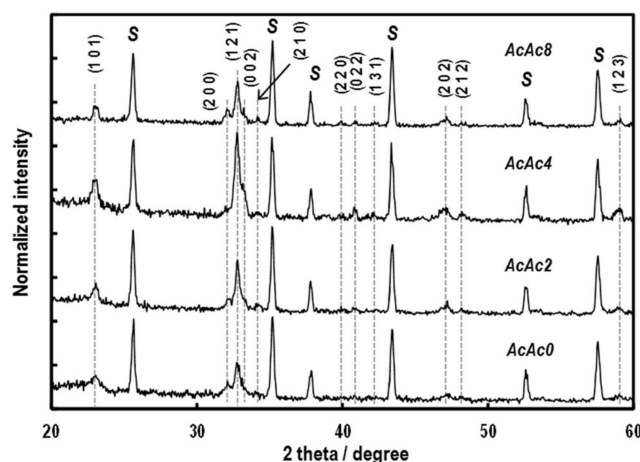


Figure 5. XRD patterns of the  $\text{SmFeO}_3$  thin-films prepared from AcAc0, 2, 4 and 8 precursors at 750 °C.

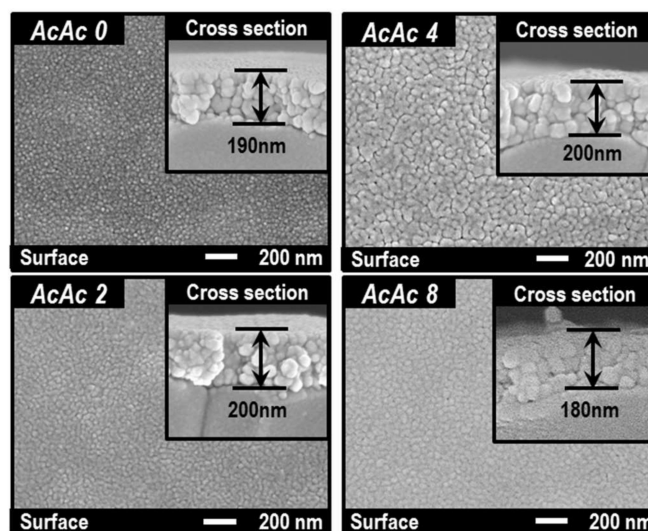
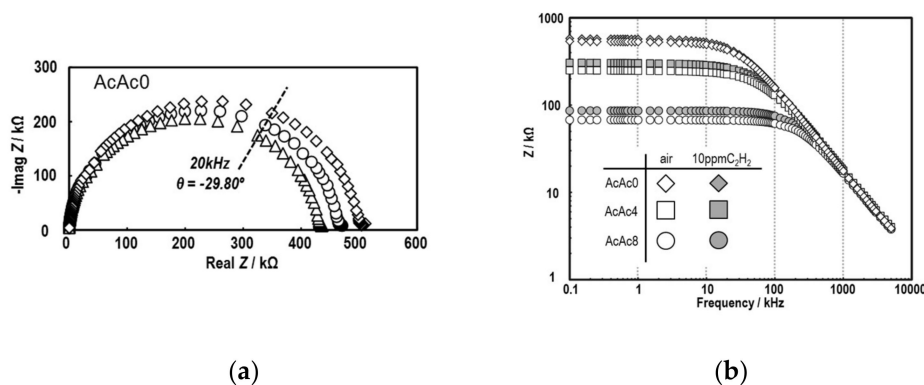


Figure 6. SEM images of the  $\text{SmFeO}_3$  thin-films prepared from AcAc0, 2, 4 and 8 precursors at 750 °C.

### 3.3. Sensing Properties of the $\text{SmFeO}_3$ Thin-Film Devices

As it is important to evaluate the frequency properties of a device in AC impedance measurement, the resistance components of a sensor using polycrystalline ceramics with bulk, grain boundary and electrode interfaces could be identified by setting a frequency. Figure 7 shows Nyquist and Bode plots of the  $\text{SmFeO}_3$  thin-films prepared by AcAc0, 2, 4 and 8 precursors at 400 °C. The Nyquist plots of the  $\text{SmFeO}_3$  thin-film by the AcAc0 precursor showed a capacitance semicircle with a negative phase angle. It could be found that the  $\text{SmFeO}_3$  thin-film has a p-type semiconductive property due to the fact that its impedance decreased entirely when the atmosphere was switched from  $P_{\text{O}_2} = 0.21$  atm to 0.75 atm [25]. On the other hand, the  $\text{SmFeO}_3$  device showed increasing impedance at 10 ppm  $\text{C}_2\text{H}_2$ . Bode plots of the  $\text{SmFeO}_3$  thin-films by AcAc0–8 precursors had some feature points. Firstly, the impedance of the device showed a constant value at a lower frequency and a stepwise decrease at a higher frequency. Secondly, the impedance of the devices decreased entirely in air by increasing AcAc. Finally, the devices with more AcAc had an increased rate of impedance to  $\text{C}_2\text{H}_2$ , especially at a low frequency. The reason why the thin-films with or without AcAc showed such behaviors should be that the thin-films that became more crystalline with AcAc had a lower potential among grains. To study the temperature dependencies of bulk and grain boundary resistance to  $\text{C}_2\text{H}_2$ , Nyquist plots from

the  $\text{SmFeO}_3$  thin-film devices at 300–500 °C were divided from bulk and grain boundaries by fitting. The sensor resistances were plotted against measurement temperature, as shown in Figure 8. It was found that the grain boundary of the AcAc8 film showed a strong dependence on temperature, and changed resistance largely at 10 ppm  $\text{C}_2\text{H}_2$ . Therefore, the  $\text{SmFeO}_3$  thin-film from the AcAc precursor has superior properties for an AC sensing material.



**Figure 7.** Nyquist plot in air (a) and Bode diagram in air and 10 ppm  $\text{C}_2\text{H}_2$  (b) of the  $\text{SmFeO}_3$  device prepared from AcAc0, 4 and 8 precursors at 400 °C.

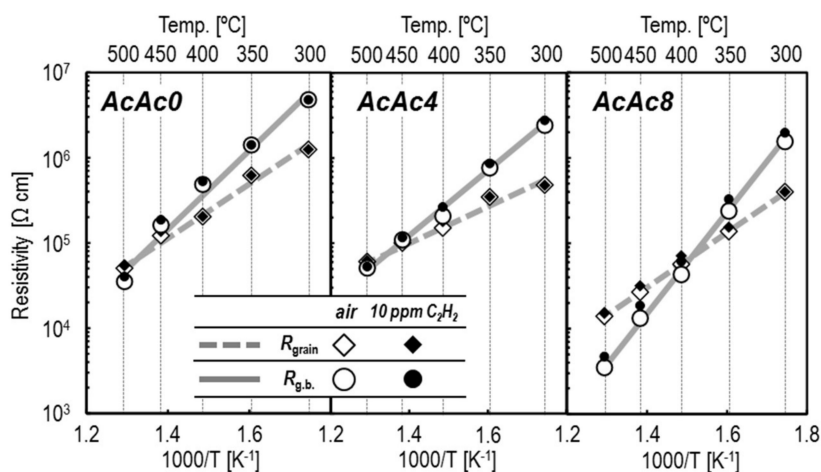


**Figure 8.** Temperature dependencies of resistivity of grain and grain boundary [g.b.] for the  $\text{SmFeO}_3$  thin-film devices at 300–500 °C.

Figure 9 shows the responses of the  $\text{SmFeO}_3$  thin-film devices to 5–15 ppm  $\text{C}_2\text{H}_2$  at 400 and 500 °C at 20 kHz. None of the devices detected  $\text{C}_2\text{H}_2$  in capacitance  $C$ , but they responded clearly in resistance  $R$ . The reason why capacitance of the devices did not show responses might be derived from the low conductivity and effect of ambient noise. With increasing the amount of additive AcAc,  $R$  of the devices decreased and became more stable. Moreover, sensor response and recovery speed were improved with increasing measurement temperature. Temperature dependencies of resistance response  $S_R$  to 5 ppm  $\text{C}_2\text{H}_2$  at 300–500 °C are shown in Figure 10. Here, the sensor response  $S_R$  was defined as in  $S_R = (R_{\text{gas}} - R_{\text{air}}) / R_{\text{air}} \times 100\%$ , where  $R$  is the resistance component in air or sample gas, written in subscript as air and gas, respectively. The temperature that the maximum response was obtained at was ca. 400–450 °C, and the AcAc8 thin-film device showed the highest response. This implies that the prepared devices have roughly equal chemical activity, and gas diffusion might be working effectively due to this result [26].

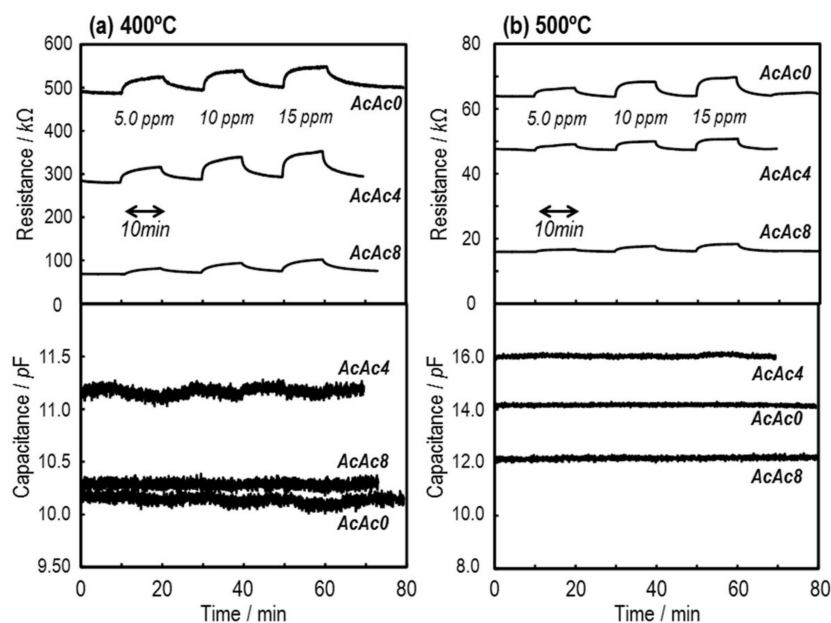


**Figure 9.** Response transients in resistance  $R$  and capacitance  $C$  components of the  $\text{SmFeO}_3$  thin-film devices prepared from AcAc0, 4 and 8 precursors to 5–15 ppm  $\text{C}_2\text{H}_2$  at (a) 400 and (b) 500 °C at 20 kHz.

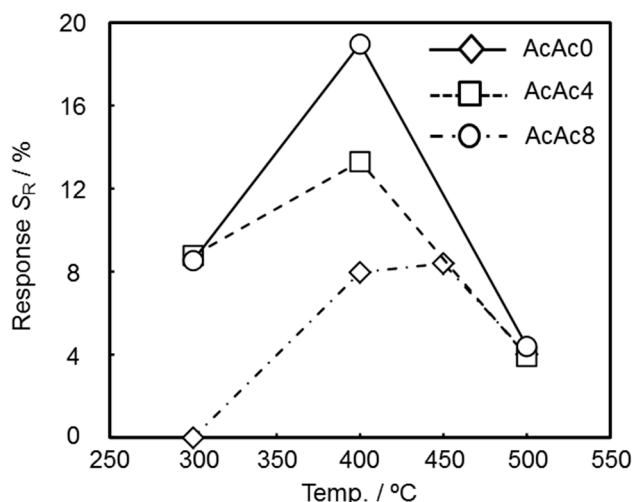


**Figure 10.** Temperature dependencies of  $S_R$  for the  $\text{SmFeO}_3$  devices at 5 ppm  $\text{C}_2\text{H}_2$  at 20 kHz.

Response transients and concentration dependencies of the  $\text{SmFeO}_3$  thin-film device AcAc8 at a low  $\text{C}_2\text{H}_2$  concentration at 400 °C, 20 kHz are shown in Figure 11. The response properties of the device at 1 MHz, which took a bulk component to compare the results of frequency, are shown simultaneously in Figure 11. The response curve at 1 MHz showed a small resistance change of about 0.8 kΩ at 2 ppm  $\text{C}_2\text{H}_2$ . The response curve at 20 kHz, however, showed a larger and faster response at 0.5 ppm  $\text{C}_2\text{H}_2$ . According to Figure 11, the  $\text{SmFeO}_3$  thin-film AcAc8 indicated the ability to be a lower- $\text{C}_2\text{H}_2$ -concentration sensor, because the device showed a relatively stable response with a moderate drift.

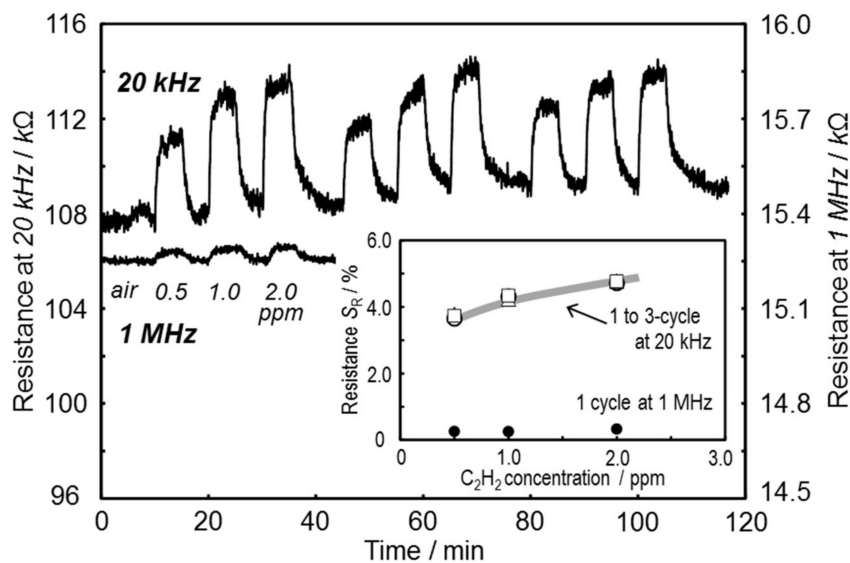


**Figure 11.** Response transient and concentration dependencies (insert) of the  $\text{SmFeO}_3$  thin-film device prepared from AcAc8 precursor to low  $\text{C}_2\text{H}_2$  concentration at  $400^\circ\text{C}$ , 20 kHz and 1 MHz.

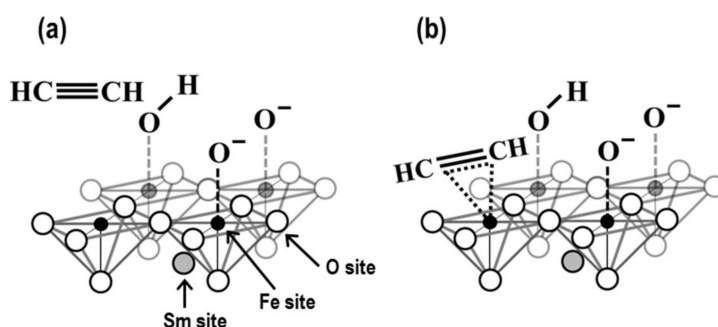


**Figure 12.** Schematic of the surface of perovskite-type oxide and appearance of adsorbed  $\text{C}_2\text{H}_2$  on an active site of perovskite; (a) before and (b) after adsorption.

The electrical state of a B-site metal ion on a perovskite-type oxide might affect sensor properties because the sensor used for Fe-based perovskite-type oxides has shown a good response differentially [16]. The sensor response in this study might tentatively have progressed via chemisorbing  $\text{C}_2\text{H}_2$  on an  $\text{Fe}^{3+}$  site, as shown in Figure 12. The  $\text{Fe}^{3+}$  of the  $\text{SmFeO}_3$  forms a six-coordinate complex in an octahedral-structured  $\text{FeO}_6$  and  $[(t_{2g})^3(e_g)^2]$  in a high-spin state. Here,  $d_{x^2-y^2}$  and  $d_{z^2}$  orbitals, which form a bond with oxygen, move into a high-energy state, and  $d_{xy}$ ,  $d_{yz}$  and  $d_{xz}$  orbitals, which have no bond, move into a low-energy state. Quintuple orbitals of Fe 3d eventually separate by forming octahedral  $\text{FeO}_6$ . The Fe 4s orbital also loses an electron to lead to a vacant orbital by oxidizing from  $\text{Fe}^{(0)}$  to  $\text{Fe}^{3+}$ . Therefore, the 3d and the 4s orbitals are HOMO and LUMO, respectively. On the other hand, the HOMO and LUMO of the  $\text{C}_2\text{H}_2$  molecule are  $\pi$  and  $\pi^*$  orbitals, respectively. To chemisorb  $\text{C}_2\text{H}_2$  on  $\text{Fe}^{3+}$ , it should be understood that an electronic interaction must occur between the HOMO and LUMO of each species [27]. When an electron that is evolved from an adsorbed oxygen is diminished by a hole in the  $\text{SmFeO}_3$  surface, this decreases conductivity of the oxide surface [28,29]. Therefore, it should be important for the  $\text{SmFeO}_3$  sensor device to have as much  $\text{Fe}^{3+}$  as possible on the surface [30].

Figure 13 shows Fe 2p and O 1s spectra of the SmFeO<sub>3</sub> thin-films of AcAc0, 2, 4 and 8. The Fe 2p<sub>3/2</sub> showed a peak at 709.9 eV which corresponds to Fe<sup>2+</sup> and Fe<sup>3+</sup> cations. The O<sub>1s</sub> also implies lattice oxygen and adsorbed oxygen at 528.9 and 531.1 eV, respectively. It might be found that there is no surface oxidation state change for each SmFeO<sub>3</sub> thin-film. Table 1 summarizes the contents of various elements on the surfaces of the AcAcX thin-films. Both elements showed an increase and decrease from semi-quantitative analysis, and relativity was not obtained between the XPS results and the sensor responses to C<sub>2</sub>H<sub>2</sub>. Therefore, this could explain that the gas diffusion properties of the SmFeO<sub>3</sub> thin-film improved the response to C<sub>2</sub>H<sub>2</sub>. Quantitative analyses and theoretical approaches are in progress to identify the sensing mechanism.

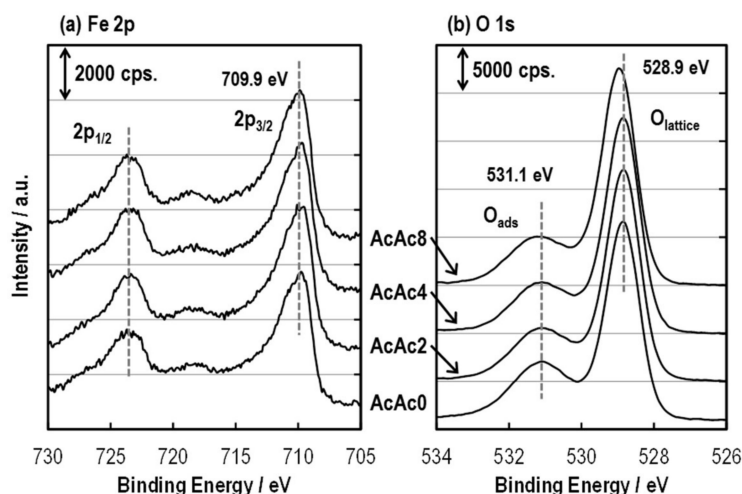


**Figure 13.** XPS spectra of the SmFeO<sub>3</sub> thin-film device prepared from AcAc0, 2, 4 and 8 precursors sintered at 750 °C; (a) Fe 2p and (b) O 1s.

**Table 1.** Ratios of the elements on the surface of the SmFeO<sub>3</sub> thin-film prepared from AcAc0, 2, 4 and 8 precursors sintered at 750 °C.

X in AcAcX	$\frac{\text{Fe}}{\text{Sm+Fe}}$	$\frac{\text{O}_{\text{lat}}}{\text{Sm+Fe}}$	$\frac{\text{O}_{\text{ads}}}{\text{Sm+Fe}}$	$\frac{\text{O}_{\text{lat}}+\text{O}_{\text{ads}}}{\text{Sm+Fe}}$
0	0.188	0.143	0.076	0.219
2	0.164	0.137	0.065	0.202
4	0.193	0.135	0.054	0.189
8	0.170	0.134	0.057	0.191

#### 4. Conclusions

The impedancemetric C<sub>2</sub>H<sub>2</sub> sensor was fabricated by using SmFeO<sub>3</sub> thin-films prepared by a polymer precursor method. Crystalline and particle growth of the SmFeO<sub>3</sub> thin-films could be controlled by the additive amount of AcAc in the solution with EG and metal nitrates. It could be illustrated by TG–DTA, FT–IR and UV–Vis that a high-coordination structure formed between metal cations and carboxylic oxygen. This affected the pyrolytic and sintering behaviors. The obtained SmFeO<sub>3</sub> thin-films showed different responses to C<sub>2</sub>H<sub>2</sub>. Moreover, the SmFeO<sub>3</sub> thin-film prepared by the AcAc8 precursor, which has good interface characteristics for a sensor, showed the best response to C<sub>2</sub>H<sub>2</sub> by means of AC impedance.

**Author Contributions:** T.T., S.T., Y.S. conceived and designed the material and set-up method; T.T. analyzed the data and wrote the paper; S.T. contributed with data delivery, and Y.S. assisted in writing the manuscript.

**Funding:** This work was partially financial supported by Nissan Science Foundation.

**Acknowledgments:** The authors are grateful for the Center for Instrumental Analysis, Kyushu Institute of Technology for XRD, XPS and FE-SEM measurements.

**Conflicts of Interest:** The authors declare no conflict of interest.

## References

1. Pimtong-Ngam, Y.; Jiemsirilers; Supothina, S. Preparation of tungsten oxide–tin oxide nanocomposites and their ethylene sensing characteristics. *Sens. Actuators A Phys.* **2007**, *139*, 7–11. [[CrossRef](#)]
2. Zevenbergen, M.A.G.; Wouter, D.; Dam, V.-A.T.; Brongersma, S.H.; Crego-Calama, M. Electrochemical Sensing of Ethylene Employing a Thin Ionic-Liquid Layer. *Anal. Chem.* **2011**, *83*, 6300–6307. [[CrossRef](#)] [[PubMed](#)]
3. Li, C.; Su, Y.; Lv, X.; Xia, H.; Wang, Y. Electrochemical acetylene sensor based on Au/MWCNTs. *Sens. Actuators B Chem.* **2010**, *149*, 427–431. [[CrossRef](#)]
4. Qi, Q.; Zhang, T.; Zheng, X.; Fan, H.; Liu, L.; Wang, R.; Zeng, Y. Electrical response of Sm<sub>2</sub>O<sub>3</sub>-doped SnO<sub>2</sub> to C<sub>2</sub>H<sub>2</sub> and effect of humidity interference. *Sens. Actuators B Chem.* **2008**, *134*, 36–42. [[CrossRef](#)]
5. Zhang, L.; Zhao, J.; Zheng, J.; Li, L.; Zhu, Z. Hydrothermal synthesis of hierarchical nanoparticle-decorated ZnO microdisks and the structure-enhanced acetylene sensing properties at high temperatures. *Sens. Actuators B Chem.* **2011**, *158*, 144–150. [[CrossRef](#)]
6. Matsumoto, H.; Tanji, T.; Amezawa, K.; Kawada, T.; Uchimoto, Y.; Furuya, Y.; Sakai, T.; Matsuka, M.; Ishihara, T. Nanoprotonics in perovskite-type oxides: Reversible changes in color and ion conductivity due to nanoionics phenomenon in platinum-containing perovskite oxide. *Solid State Ionics* **2011**, *182*, 13–18. [[CrossRef](#)]
7. Meadowcroft, D.B. Low-cost carbon monoxide electrode material. *Nature* **1970**, *226*, 847–848. [[CrossRef](#)]
8. Itagaki, Y.; Mori, M.; Hosoya, Y.; Aono, H.; Sadaoka, Y. O<sub>3</sub> and NO<sub>2</sub> sensing properties of SmFe<sub>1-x</sub>Co<sub>x</sub>O<sub>3</sub> perovskite oxides. *Sens. Actuators B Chem.* **2007**, *122*, 315–320. [[CrossRef](#)]
9. Tomoda, M.; Okano, S.; Itagaki, Y.; Aono, H.; Sadaoka, Y. Air quality prediction by using semiconducting gas sensor with newly fabricated SmFeO<sub>3</sub> film. *Sens. Actuators B Chem.* **2004**, *97*, 190–197. [[CrossRef](#)]
10. Chaudhari, G.N.; Jagtap, S.V.; Gedam, N.N.; Pawar, M.J.; Sangawar, V.S. Sol-gel synthesized semiconducting LaCo<sub>0.8</sub>Fe<sub>0.2</sub>O<sub>3</sub>-based powder for thick film NH<sub>3</sub> gas sensor. *Talanta* **2009**, *78*, 1136–1140. [[CrossRef](#)]
11. Chai, Y.L.; Ray, D.T.; Chen, G.J.; Chang, Y.H. Synthesis of La<sub>0.8</sub>Sr<sub>0.2</sub>Co<sub>0.5</sub>Ni<sub>0.5</sub>O<sub>3-δ</sub> thin films for high sensitivity CO sensing material using the Pechini process. *J. Alloys Compd.* **2002**, *333*, 147–153. [[CrossRef](#)]
12. Sahner, K.; Moos, R.; Matam, M.; Tunney, J.J.; Post, M. Hydrocarbon sensing with thick and thin film p-type conducting perovskite materials. *Sens. Actuators B Chem.* **2005**, *108*, 102–112. [[CrossRef](#)]
13. Liu, X.; Hu, J.; Cheng, B.; Qin, H.; Zhao, M.; Yang, C. First-principles study of O<sub>2</sub> adsorption on the LaFeO<sub>3</sub> (0 1 0) surface. *Sens. Actuators B Chem.* **2009**, *139*, 520–526. [[CrossRef](#)]
14. Sun, L.; Hu, J.; Zhang, L.; Gao, F.; Zhang, Y.; Qin, H. Adsorption of CO on the O<sub>2</sub> pre-adsorbed LaFeO<sub>3</sub> (0 1 0) surface: A density functional theory study. *Curr. Appl. Phys.* **2011**, *11*, 1278–1281. [[CrossRef](#)]
15. Sun, L.; Hu, J.; Qin, H.; Zhao, M.; Fan, K. Influences of Ca doping and oxygen vacancy upon adsorption of CO on the LaFeO<sub>3</sub> (010) surface: A first-principles study. *J. Phys. Chem. C* **2011**, *115*, 5593–5598. [[CrossRef](#)]
16. Tasaki, T.; Takase, S.; Shimizu, Y. Fabrication of Sm-Based Perovskite-Type Oxide Thin-Films and Gas Sensing Properties to Acetylene. *J. Sens. Technol.* **2012**, *02*, 75–81. [[CrossRef](#)]
17. Tasaki, T.; Takase, S.; Shimizu, Y. Impedancemetric acetylene gas sensing properties of Sm-Fe-based perovskite-type oxide-based thick-film device. *Sens. Actuators B Chem.* **2013**, *187*, 128–134. [[CrossRef](#)]
18. Karageorgakis, N.I.; Heel, A.; Bieberle-Hütter, A.; Rupp, J.L.M.; Graule, T.; Gauckler, L.J. Flame spray deposition of La<sub>0.6</sub>Sr<sub>0.4</sub>CoO<sub>3-δ</sub> thin films: Microstructural characterization, electrochemical performance and degradation. *J. Power Sources* **2010**, *195*, 8152–8161. [[CrossRef](#)]
19. Ueno, K.; Sakamoto, W.; Yogo, T.; Hirano, S. Synthesis of conductive LaNiO<sub>3</sub> thin films by chemical solution deposition. *Japanese J. Appl. Physics, Part 1 Regul. Pap. Short Notes Rev. Pap.* **2001**, *40*, 6049–6054. [[CrossRef](#)]
20. Shimizu, Y.; Murata, T. Sol-gel synthesis of perovskite-type lanthanum manganite thin films and fine powders using metal acetylacetonate and poly(vinyl alcohol). *J. Am. Ceram. Soc.* **1997**, *80*, 2702–2704. [[CrossRef](#)]
21. Aono, H.; Tomida, M.; Sadaoka, Y. Conventional synthesis method for fine polycrystalline LaFeO<sub>3</sub> using ethylene glycol solvent addition. *J. Ceram. Soc. Japan* **2009**, *117*, 1048–1051. [[CrossRef](#)]
22. Choppali, U.; Kougianos, E.; Mohanty, S.P.; Gorman, B.P. Polymeric precursor derived nanocrystalline ZnO thin films using EDTA as chelating agent. *Sol. Energy Mater. Sol. Cells* **2010**, *94*, 2351–2357. [[CrossRef](#)]
23. Miller, J.B.; Ashok, T.; Lee, S.; Broitman, E. Zinc oxide-based thin film functional layers for chemiresistive sensors. *Thin Solid Films* **2012**, *520*, 6669–6676. [[CrossRef](#)]

24. Keyes, B.M.; Gedvilas, L.M.; Li, X.; Coutts, T.J. Infrared spectroscopy of polycrystalline ZnO and ZnO:N thin films. *J. Cryst. Growth* **2005**, *281*, 297–302. [[CrossRef](#)]
25. Carotta, M.C.; Martinelli, G.; Sadaoka, Y.; Nunziante, P.; Traversa, E. Gas-sensitive electrical properties of perovskite-type SmFeO<sub>3</sub> thick films. *Sens. Actuators B Chem* **1998**, *B48*, 270–276. [[CrossRef](#)]
26. Vuong, D.D.; Sakai, G.; Shimano, K.; Yamazoe, N. Hydrogen sulfide gas sensing properties of thin films derived from SnO<sub>2</sub> sols different in grain size. *Sens. Actuators B Chem* **2005**, *105*, 437–442. [[CrossRef](#)]
27. Hoffmann, R.; Chen, M.M.-L.; Thorn, D.L. Qualitative Discussion of Alternative Coordination Modes of Diatomic Ligands in Transition Metal Complexes. *Inorg. Chem.* **1977**, *16*, 503–511. [[CrossRef](#)]
28. Barsan, N.; Koziej, D.; Weimar, U. Metal oxide-based gas sensor research: How to? *Sens. Actuators B Chem* **2007**, *121*, 18–35. [[CrossRef](#)]
29. Yamazoe, N.; Shimano, K. New perspectives of gas sensor technology. *Sens. Actuators B Chem* **2009**, *138*, 100–107. [[CrossRef](#)]
30. Zhang, R.; Villanueva, A.; Alamdari, H.; Kaliaguine, S. Cu- and Pd-substituted nanoscale Fe-based perovskites for selective catalytic reduction of NO by propene. *J. Catal.* **2006**, *237*, 368–380. [[CrossRef](#)]



© 2019 by the authors. Licensee MDPI, Basel, Switzerland. This article is an open access article distributed under the terms and conditions of the Creative Commons Attribution (CC BY) license (<http://creativecommons.org/licenses/by/4.0/>).